 DOI 10.1002/mawe.201000593 

# Elastic finite element analysis on cross-sections of random hollow sphere structures

## Elastische Finite-Elemente-Analyse von Querschnitten zufällig angeordneter Hohlkugelstrukturen

T. Fiedler[1,2], H. S. Kim[2], I. V. Belova[1,2], S. W. Sloan[1,2], G. E. Murch[1,2], A. Öchsner[2,3]

**This paper addresses elastic analysis based on 2D finite element models for metallic hollow-sphere structures. In the first part, the influence of micro-porosity on the elastic behaviour of sintered metallic hollow sphere wall material is investigated. Young's modulus of the metallic hollow sphere wall material is found to linearly decrease with increasing micro-porosity ranging up to about 45%. In the second part, elastic parameters for metallic syntactic foams (MSF) consisting of thin or thick walled hollow spheres, and for epoxy containing spherical pores are studied. Data obtained from finite element models are compared with theoretical predictions based on the rule of mixtures developed elsewhere and found to be in good agreement with each other for MSF but not for porous epoxy. The shear modulus of MSF with thin-walled hollow spheres was found to increase with increasing volume fraction of matrix whereas that of MSF with thick walled hollow spheres was found to decrease. Specific Young's modulus of MSF with thin-walled hollow spheres was also found to increase with increasing foam density whereas that of MSF with thick walled hollow spheres was found to decrease. Poisson's ratio obtained was relatively low for porous epoxy matrix material but high for MSF with thin or thick-walled hollow spheres.**

**Keywords:** finite element analysis / cellular metal / hollow spheres / syntactic foam / elastic properties

**Dieser Artikel beschäftigt sich mit der elastischen Finite-Elemente- Analyse zwei-dimensionaler Modelle von Hohlkugelstrukturen. Im ersten Teil der Arbeit wird der Einfluss von Mikroporosität auf das elastische Verhalten der gesinterten Hohlkugelschale untersucht. Es wurde beobachtet, dass der Elastizitätsmodul des gesinterten Materials linear mit steigender Porosität abnimmt. Der zweite Teil der Arbeit befasst sich mit Hohlkugelstrukturen bestehend aus Hohlkugeln und Epoxidmatrix verschiedener Wandstärken $t$: dickwandige Hohlkugeln, dünnwandige Hohlkugeln und dem Grenzfall $t \to 0$ (kugelförmige Einschlüsse ohne Hohlkugelschale). Die Ergebnisse der Finite-Elemente-Analyse wurden mit analytischen Modellen verglichen und mit Ausnahme der kugelförmigen Einschlüsse eine gute Übereinstimmung erzielt. Der Schubmodul dünnwandiger Hohlkugelstrukturen nimmt mit zunehmendem Volumenanteil der Epoxidmatrix zu, der Schubmodul von dickwandigen Hohlkugelstrukturen jedoch ab. Die ermittelten Querkontraktionszahlen sind für den Fall kugelförmiger Einschlüsse ($t \to 0$) vergleichsweise niedrig. Deutlich höhere Ergebnisse wurden für dünn- und dickwandige Hohlkugelstrukturen erzielt.**

**Schlüsselwörter:** Finite-Elemente-Analyse / zellulares Metall / Hohlkugeln / syntaktischer Schaum / elastische Eigenschaften

## 1 Introduction

Hollow sphere structures include composites consisting of hollow spheres and matrix. The composites may be classified into two categories depending on volume content of hollow spheres or matrix. When they are made of a high volume content of matrix, they may be referred to as hollow sphere modified particulate composites, whereas when they are made of a high volume content of hollow spheres, they may be referred to as syntactic foams [1]. The demarcation between the two categories in terms of volume content may be arbitrary. However, hollow spheres in the former are usually more for toughening the matrix while those in the latter are more for stiffness and density [1, 2].

[1] Priority Research Center for Geotechnical and Materials Modelling, The University of Newcastle, Callaghan, NSW 2308, Australia
[2] School of Engineering, The University of Newcastle, Callaghan, NSW 2308, Australia
[3] Department of Applied Mechanics, Faculty of Mechanical Engineering, Technical University of Malaysia, 81310 UTM Skudai, Johor, Malaysia

Correspondence author: T. Fiedler, Priority Research Centre for Geotechnical and Materials Modelling, School of Engineering, The University of Newcastle, Callaghan, NSW 2308, Australia
**E-mail:** Thomas.Fiedler@newcastle.edu.au

  

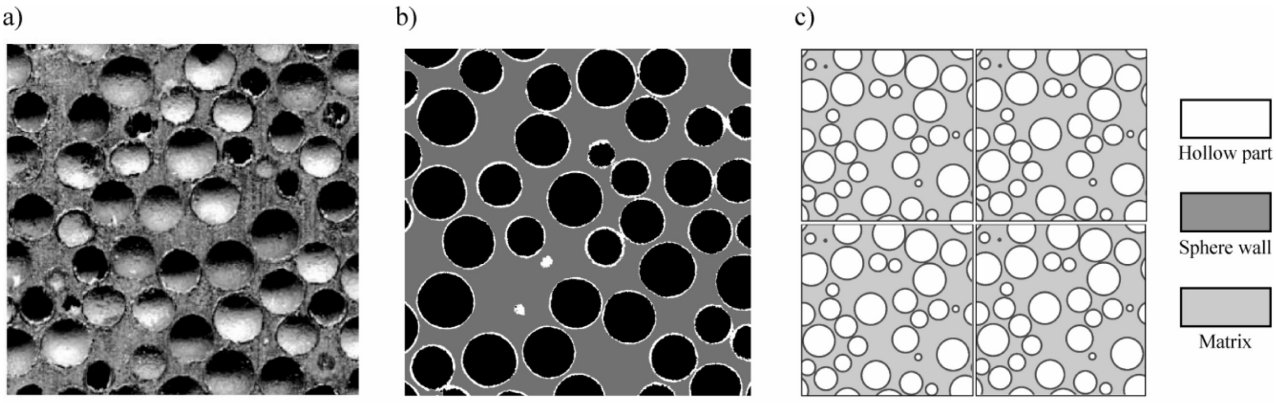


**Fig. 1.** Cross-sections of a syntactic foam consisting of mono-sized hollow spheres at random positions and matrix: a) photograph of real image, b) computed tomography reconstruction, c) computer-generated models.

**Abb. 1.** Querschnitte syntaktischer Schäume bestehend aus gleichartigen Hohlkugeln und Epoxidmatrix: a) Photographie, b) Computertomographische Rekonstruktuion, c) Computer-generierte Modelle.

Syntactic foams can be used in various structural components including sandwich composites [3, 4] and in areas where low densities are required e. g. undersea/marine equipment for deep ocean current-metering, anti-submarine warfare [5, 6, 7, 8, 9]. When they are used as core materials for sandwich composites, they contribute to an increase in specific stiffness. They further contribute not only to the reduction in damage but also to the prevention of failure of composite systems by inducing their own damage when used for protective structural components [10]. Their other uses include products in aerospace and automotive industries [11].

A wide range of different types of syntactic foams made of ceramic hollow microspheres can be made by selecting different materials and consolidating techniques for binder and hollow microspheres. The consolidating techniques include coating microspheres [12], rotational moulding [13], extrusion [14, 15] and techniques which use inorganic binder solution and firing [16], dry resin powder for sintering [17, 18, 19, 20], compaction [21, 22], liquid resin as binder [23] for *in situ* reaction injection moulding, buoyancy [10, 24, 25], casting [26] and pressure infiltration [27]. Recently, a new type of syntactic foams has been developed through sintering process for metallic hollow sphere structures [28], which will be referred to here as metallic syntactic foams (MSF). MSFs are manufactured by pouring single hollow spheres into a mould and adding an epoxy resin for binding. They are capable of possessing tailored properties for deformation particularly under impact conditions, good structural and acoustic damping properties, high specific stiffness and strength, and low thermal conductivities [29, 30]. The hollow sphere geometry in MSF is easily reproducible and therefore mechanical and physical properties are better controllable than conventional cellular metals. It was shown in [31] that MSF can be considered isotropic to a good approximation. Finite element analysis for such MSF may be useful for optimization of volume fractions of constituents for elastic behaviour. However, little work has been found in the literature for such analysis.

In this paper, 2D finite element analyses on the MSF consisting of metallic hollow spheres and epoxy as matrix, and also hollow spheres as structures affected by porosity within sphere wall due to sintering process are conducted for elastic behaviour affected by mixing ratio of the constituents.

## 2 Finite Element Modeling

Two different types of 2D finite element models were employed in this paper. The first type of model is to represent porous structures consisting of solid and void phases. It was used for analysis of sintered hollow-sphere wall material affected by micro-porosity. To this end, a solid volume ($V$) was chosen and small pores were inserted at random sites. Models with various porosities (i. e. total volume occupied by micro-pores divided by the initial volume $V$) ranging between 0 (solid material) and 0.45 were generated. The maximum possible porosity of this analysis is given by the limit where the two-dimensional model loses its connectivity and disintegrates. The hollow sphere wall in the second type of models (see below) was modeled as a solid and the material properties obtained for the micro-porosity models were assigned to this material.

The second type of model is to represent MSFs comprising cross-sections of *hollow spheres* and matrix. *Figure 1* shows various images for cross-sections of a MSF, generated from different sources, consisting of nominally mono-sized hollow spheres at random positions, and matrix. Figure 1a is from a photograph of a real image, Fig. 1b from computed tomography reconstruction, Fig. 1c from computer-generated models for analysis. Three different phases can be identified i. e. matrix, hollow sphere, and voids in both sphere wall and hollow part. The residual micro-porosity (after the sintering) within the sphere wall after manufacturing is not shown here due to the limitation of resolution in the models of the cross-sections. The analyses using models (Fig. 1b and 1c) are for the approximate characterization of a complex three dimensional material. Recent results [32] indicate that the model approach would only be achieved if the considered geometry is representative of a sufficiently large size. In order to investigate the applicability of

 

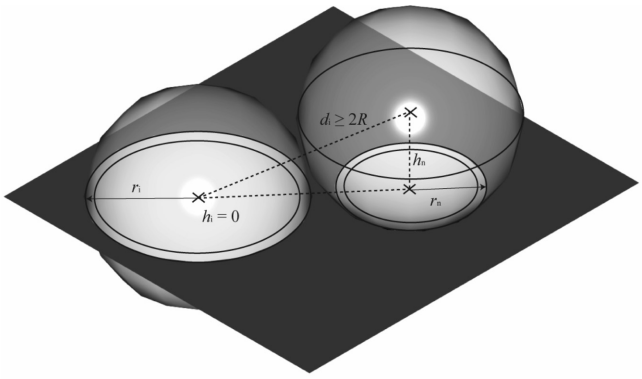


**Fig. 2.** Adding of circles in the cutting plane.

**Abb. 2.** Hinzufügen von Kreisen innerhalb einer Schnittebene.

this approach, numerical results will be compared with experimental data and analytical solutions.

The advantage of modeling based on the tomography (Fig. 1b) is the representation of the accurate geometry of a real cross-section of a MSF obtained by scanning. However, the disadvantage is that the variation of geometric parameters is difficult to achieve, and the size and resolution of the geometry are limited by the computed tomography data. In contrast, randomly generated cross sections (Fig. 1c) allow for an aimed variation of geometric parameters such as volume fraction and wall thickness. Also, the model size is only limited by the available computer hardware capacity so that larger geometries with a higher resolution would be applicable.

The outer radii ($R$) of the metallic hollow spheres and the sphere wall thicknesses in the computed tomography images are approximately 1.5 mm and 0.075 mm respectively. It is noted that radii ($r_i$) (*Fig. 2*) of their circular cross sections depend on the distance ($h_i$) of their centre points to the cutting plane and are given by $R_i(h_i) = \sqrt{R^2 - h_i^2}$.

*Some* of the calculation models were directly derived from cross-sections obtained by computed tomography scans (Fig. 1b). The chosen alternative to computed tomography data is the usage of random-generated calculation models that allow for a controlled variation of geometric parameters. As an example, the influence of the sphere wall thickness on the structure's elastic properties is investigated. Three different cases were considered i. e. the limiting case without sphere wall (only matrix and pores), a thin wall ($t$ = 0.075 mm = 0.05 $R$) and a thick wall ($t$ = 0.15 mm = 0.1 $R$). The area fraction (representing volume fraction) of the matrix was changed by varying the number of hollow spheres. The computer-generated models were created using an algorithm which sequentially fills spheres into a grid at randomly selected coordinates $C_i(Xi, Y_i, h_i)$. It allows the distance ($h_i$) (Fig. 2) to be smaller than the sphere radius ($R$) in order to obtain the cross section. Further, it defines the position ($p_i$) of the centre point ($C_i$) relative to the cutting plane (i. e. below: $p_i = 1$, above: $p_i = -1$). In the following algorithm, any intersection of the last added sphere in relation with pre-existing spheres is checked. Therefore, the distances ($d_i$) between the spheres are calculated according to:

$$d_i = \sqrt{(X_n - X_i)^2 + (Y_n - Y_i)^2 + (p_n \cdot h_n - p_i \cdot h_i)^2} (i = 1 \infty n - 1). \quad (1)$$

Whenever any distance $d_i$ is smaller than two times the sphere radius ($R$), the last added sphere $n$ was removed because at least two spheres intersect each other. Figure 2 illustrates this for the case, $h_i = 0$. Additional attempts of adding spheres were made in the model whenever intersection occurred. In the case where the number of attempts reaches $10^7$, it was assumed that no further spheres can be positioned in the gaps between previously added spheres. In order to analyse a representative cross section of the MSF, each grid contained at least 100 circles.

For the grid generation, two-dimensional matrices $\mathbf{M}(X,Y)$ with a resolution of 1000 by 1000 points were created. For each entry of $\mathbf{M}$, the distances $d(X,Y)$ between the corresponding coordinate $(X,Y,0)$ and the centre points $(X_i,Y_i,h_i)$ of the spheres were calculated according to:

$$d(X, Y) = \sqrt{(X - X_i)^2 + (Y - Y_i)^2 + h_i^2} (i = 1 \infty n). \quad (2)$$

The following three cases were defined in the grid for matrix, wall and hollow part of sphere:

$d(X, Y) > R$ — all circles } — Matrix

$d(X, Y) = R$ for $d(X,Y) > R - t$ — one circle / all circles } — Sphere wall

$d(X, Y) = R - t$ — one circle } — Hollow part

A particular cross section through MSF can be characterized by its area fractions. Thus, the sum of the area fractions for matrix ($A_M$), wall ($A_W$) and hollow part ($A_H$) is equal to unity. The area fractions on the grid were obtained by summing up the grid points allocated to each phase and then dividing them by the total amount of grid points (10002). The average density of a MSF ($\bar{\rho}$) was calculated using:

$$\bar{\rho} = A_W \cdot \rho_W + A_M \cdot \rho_M \quad (3)$$

where $\rho_M$ and $\rho_W$ are the densities of the epoxy matrix and cell wall material, respectively.

## 3 Finite Element Analysis

The finite element analysis (using the commercial MSC.Marc[1] software) was performed through three stages: pre-processing, processing, and post-processing. The pre-processing is the generation of calculation models including geometric discretisation, definition of material properties and boundary conditions. The grid models described in Section 2 were used to generate the finite element calculation meshes where one square element replaces one grid point, and material properties were defined according to the identified phases (matrix, sphere wall, hollow part). The material properties used are given in *Table 1* [44].

For elastic analysis, uni-axial compressive testing was simulated (*Fig. 3*). To this end, a time ($t$)-dependent nodal displacement $u = a \cdot t$ ($a$ = const.) was prescribed at the upper edge of the geometry. The displacement of the opposing edge is confined into $x$-direction (reflective symmetry). In order to prevent displacement in the $y$-direction, reflective symmetry conditions were also prescribed at the left side of the model. In all finite element analyses, the plain-stress state was adopted.

 

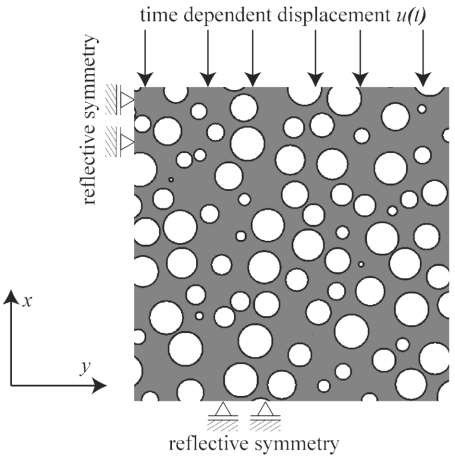


**Fig. 3.** Boundary conditions of the finite element analysis.

**Abb. 3.** Randbedingungen der Finite-Elemente-Analyse.

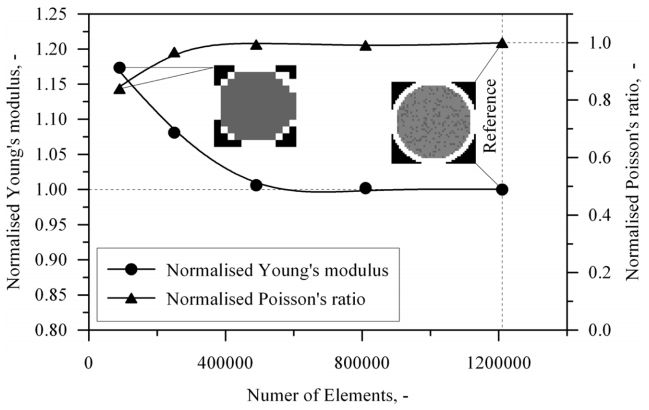


**Fig. 4.** Normalized Young's modulus versus number of elements for mesh refinement.

**Abb. 4.** Normierter Elastizitätsmodul aufgetragen über der Elementanzahl.

**Table 1.** Physical properties of constituent materials.

**Tabelle 1.** Physikalische Eigenschaften der Grundmaterialien.

| Material | Young's modulus | Shear modulus | Poisson's ratio | Density |
|---|---|---|---|---|
| Epoxy resin | 2.40 GPa | 882 MPa | 0.36 | 1.13 g/cm³ |
| Solid steel | 210 GPa | 80.77 GPa | 0.30 | 6.95 g/cm³ |
| Sintered steel | 180 GPa | 69.57 GPa | 0.29 | 6.55 g/cm³ |

Subsequent processing was conducted using the non-linear finite element solver MSC.Marc®. In the post-processing, elastic properties such as Young's modulus ($E$) and Poisson's ratio ($v$) were determined. Under the boundary conditions defined (cf. Fig. 3), Young's modulus equals the ratio of effective stresses to strains in the $x$ loading-direction. Effective values were obtained by averaging over all nodes where the nodal displacement boundary condition is prescribed:

$$E = \frac{\sigma_x}{\varepsilon_x} \tag{4}$$

where $E$ is the Young's modulus, $s$ is the stress and $e$ the strain. The Poisson's ratio ($v$) is given by the ratio of transversal $\varepsilon_y$ to longitudinal strains $\varepsilon_x$:

$$v = \frac{\varepsilon_y}{\varepsilon_x} \tag{5}$$

The shear modulus ($G$) was calculated using:

$$G = \frac{E}{2(1+v)} \tag{6}$$

As the applied voxel technique requires a fine resolution in order to map the detailed geometric information on the numerical model, a sufficient mesh density, i. e. number of finite elements, was used. Also, to minimize the numerical error, it was ensured that finite element solutions converge towards a plateau value by increasing the number of finite elements as shown in Fig. 4 for random-generated MSF cross-sections. Five different mesh densities were considered. Convergence occurs around 400,000 elements. As a result, only meshes containing $10^6$ or more elements were employed. The bitmap images of a single sphere in *Fig. 4* show the minimum and maximum geometric resolutions. It is obvious that the low resolutions are insufficient for the geometric representation.

## 4 The Rule of Mixtures for the Elastic Modulus

Mechanical behaviour of syntactic foams is generally dependent upon properties and volume fractions of constituents, and geometry of spheres such as ratio of sphere diameter to wall thickness. At a very low binder content, syntactic foams are not structurally useful and thus failure mode is mainly of gross disintegration as addressed in the literature [12, 33]. However, as the binder content increases, syntactic foams become useful as structures and further, their mechanical behaviour is affected by various conditions arising from relative properties of constituents and relativity between load carrying capacities of constituents [34, 35]. Kim and Islam [34] identified various failure conditions and hence various mixture rules for strength and elastic modulus arising from failure analysis. Two equations are given below for the elastic modulus. The first equation (7) is for large volume fractions of binder (matrix), which will be compared with numerical data in this paper, resulting in the Voigt law of mixtures under the iso-strain condition [36]:

$$G = G_{hs}(1 - v_m) + G_m v_m \tag{7}$$

where $G$ is the effective shear modulus of the composite (syntactic foam), v is the volume fraction, and subscripts ($hs$ and $m$) denote hollow sphere and matrix respectively. $G_{hs}$ in equation above is the average shear modulus where the shear stress area consists of hollow part and sphere wall cross sectional areas. The second equation is for the case where binder fails due to small volume fractions of binder with weak bonding between hollow spheres:

$$G = CG_m v_m \tag{8}$$

where $C$ is a constant. Equation (8) was found to be well correlated with experimental data [35].

 

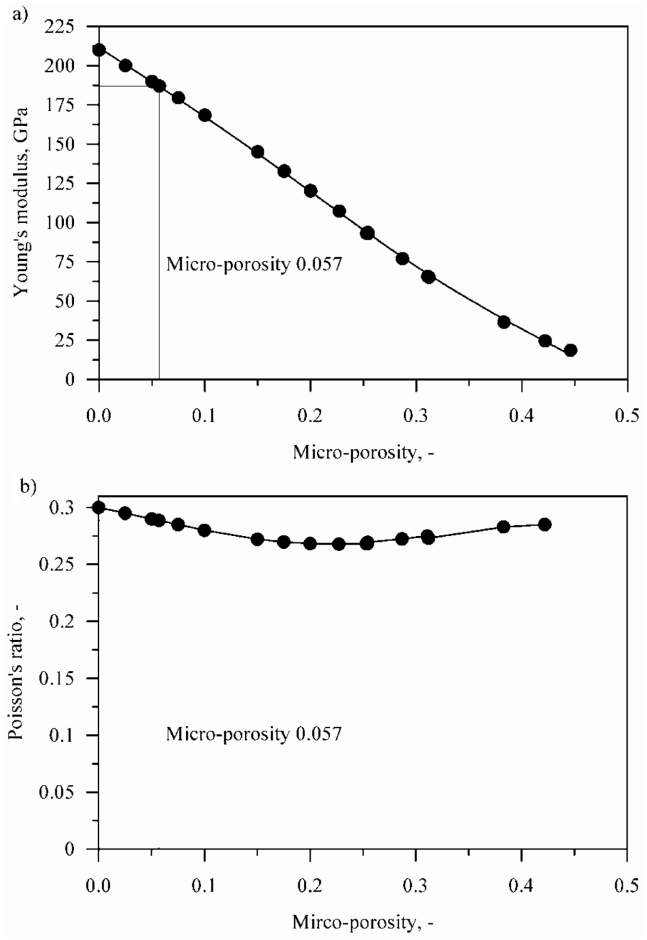


**Fig. 5.** Elastic properties of the sintered cell wall material: a) Young's modulus E, b) Poisson's ratio $\nu$.

**Abb. 5.** Elastische Eigenschaften der Hohlkugelschale: a) Elastizitätsmodul, b) Querkontraktionszahl.

It should be noted that numerous mathematical expressions based on the micro-mechanics models for particulate composites which might be relevant to syntactic foams have been developed for the elastic modulus [36, 37, 38, 39]. However, most expressions require the modulus of hollow spheres to be determined. A hollow sphere is a structure possessing a stiffness which is not a property but can be determined using the hollow sphere wall modulus. The stiffness of hollow spheres in the matrix depends on hollow sphere wall thickness and the ratio of inner to outer diameters, boundary conditions and porosity in sphere wall material. A typical expression, which will be used here for comparison, was given for a high volume fraction of matrix by Eshlby [39, 40]:

$$G = G_m\left\{1 + \frac{5(3K_m + 4G_m)(G_m - G_{hs})}{(9K_m + 8G_m)G_m + (6K_m + 12G_m)G_{hs}}(1 - \nu_m)\right\}^{-1} \quad (9)$$

where $K_m$ is the bulk modulus of matrix. The shear modulus ($G_{hs}$) in this equation will be regarded as the effective shear modulus for application for hollow spheres of MSF. For porous materials without hollow spheres ($G_{hs} = 0$), Equation (10) becomes:

$$G = G_m\{1 + 5(3K_m + 4G_m)9K_m + 8G_m(1 - \nu_m)\}^{-1} \quad (10)$$

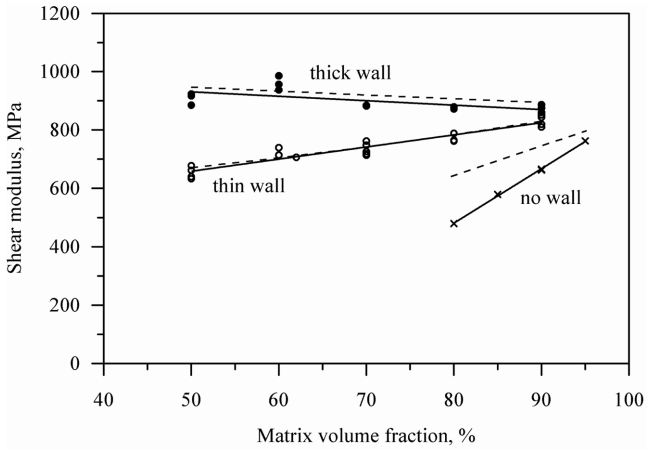


**Fig. 6.** Numerical results for shear modulus versus volume fraction of matrix. Solid lines represent Equation (6) and dashed lines Equation (8).

**Abb. 6.** Numerische Ergebnisse des Schubmoduls aufgetragen über dem Volumenanteil der Matrix. Durchgezogene Linien repräsentieren Gleichung (6), gestrichelte Linien Gleichung (8).

## 5 Results and Discussion

### 5.1 Sintered Hollow Sphere Wall Material

Elastic properties of the sintered metallic hollow sphere wall material were calculated to find the effect of the micro-porosity within the wall. Young's modulus ($E$) and Poisson's ratio ($\nu$) obtained are shown in *Fig. 5*. It can be seen that Young's modulus ($E$) is approximately a linear function of the micro-porosity although a slight deviation from the linearity is found for very high porosities (greater than 0.3). The high linearity agrees well with experimental results elsewhere [41]. Poisson's ratio appears to weakly depend upon the micro-porosity and exhibits the minimum value at a micro-porosity of 0.22. A micro-porosity of the sintered sphere wall material was determined elsewhere and given to be 0.057 [42]. Elastic parameter values corresponding to the micro-porosity (0.057) are found to be $E$ = 179.5 GPa ($G$ = 69.6 GPa) and $\nu$ = 0.29 from data given in Fig. 5, which are those already shown for MSF modeling in Table 1.

### 5.2 Metallic Syntactic Foams and Porous Material

Numerical results obtained for the elastic shear modulus from two-dimensional models of MSFs are given in *Figure 6* for three different cases. Unless stated otherwise, models of cross-sections are for those with random hollow sphere positions. The first case is for MSF (thick walled) in which the hollow sphere wall is 0.15 mm thick (= 0.1 $R$), and the second case for MSF (thin wall) in which the hollow sphere wall is 75 µm (= 0.05 $R$). The last case is for zero walled hollow spheres. The shear modulus for the thick walled case decreases as the volume fraction of binder increases, indicating that hollow spheres stiffness is relatively high compared to that of binder occupying the same volume as the hollow sphere. Thus, thick hollow spheres contribute more than the matrix to the modulus of the MSF. However, in the case of MSF

 

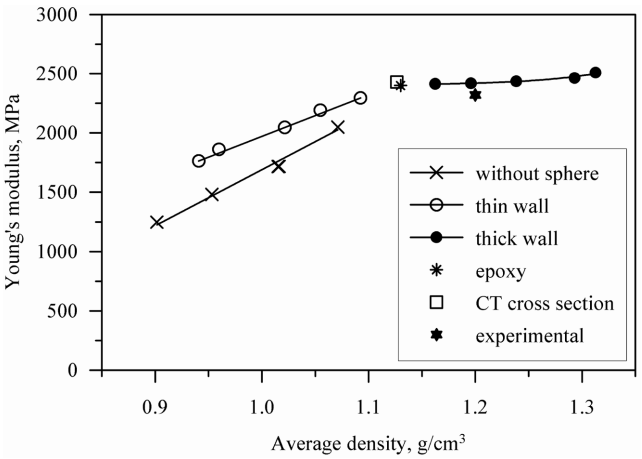


**Fig. 7.** Young's modulus as a function of average density.

**Abb. 7.** Elastizitätsmodul als Funktion der gemittelten Dichte.

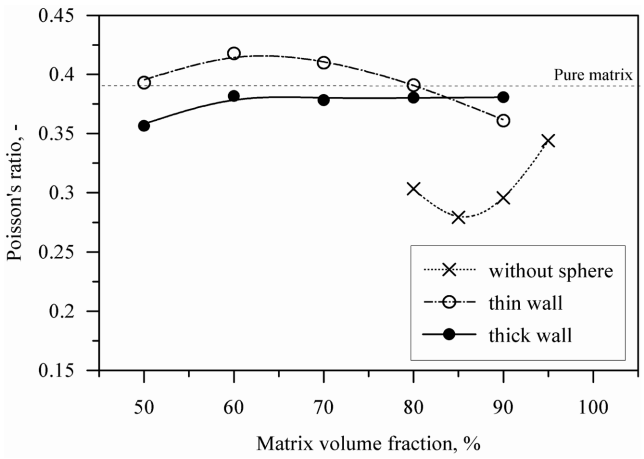


**Fig. 8.** Poisson's ratio versus matrix volume fraction.

**Abb. 8.** Querkontraktionszahl aufgetragen über dem Volumenanteil der Matrix.

with thin walled hollow spheres, its shear modulus increases as the volume fraction of matrix increases, indicating that the average effective shear modulus of hollow sphere as a structure is low compared to that of the matrix. This trend is more prominent as expected in the zero walled case. Equation (6) describes the data well with correlation factors 0.624, 0.948 and 0.999 for thick walled, thin walled and zero walled cases respectively. The low correlation factor of 0.624 seems due to the insensitivity of volume fraction of binder rather than the validity of the equation. Thus, Equation (6) appears useful and may be extended for estimating the effective shear modulus ($G_{hs}$) representing the stiffness of the hollow sphere as a structure. The estimates are found to be 1.01 GPa and 451 MPa for thick walled and thin walled hollow spheres respectively from the intercepts at zero matrix volume, supporting earlier qualitative interpretation that the stiffness of thick walled hollow spheres is high compared to that of epoxy in equivalent volume and vice versa. As for the zero walled hollow microsphere, which is the limiting case or in a different class from syntactic foams, Equation (6) correlates very well in curve fitting but it does not provide good insight into the stiffness of equivalent entity being a negative value of 1.01 GPa (= $G_{hs}$). Also Equation (8) based on micro-mechanics model using the values ($G_{hs}$ = 1.01 GPa or 451 MPa) determined from Equation (6) is shown as a dashed line in Fig. 6 for the thick walled and thin walled hollow sphere cases. It describes the shear modulus of MSF as well as Equation (6). However, it correlates poorly with data for the zero thickness walled case. The high linearity between shear modulus and volume fraction of matrix for the three different cases agrees well with experimental results given elsewhere for other hollow sphere structures [41, 43].

The Young's modulus ($E$) obtained as a function of density from finite element analyses including tomography based models is given in *Fig. 7* with data points from an experiment of MSF [44] and pure epoxy (cf. Table 1). Each data point represents an average value from five different samples. For lightweight structural applications, materials with high specific properties (e. g. modulus divided by density) are preferred for comparison of different materials. A straight line that intersects the origin in Fig. 6 can be used to locate equal specific Young's modulus values. Any higher specific Young's modulus values are located in the top left area to the straight line of equal values, and any lower specific Young's modulus values are located in the bottom right area to the straight line. Both thin (denoted by unfilled circles) and thick (denoted by filled circles) walled MSF generally exhibit higher specific Young's moduli than the zero walled case (denoted by crosses). Specific Young's modulus of a thin walled MSF appears to increase with increasing foam density whereas that of a thick walled MSF to decrease. This information indicates that the more thin walled hollow spheres and the less thick walled hollow spheres, the higher the specific Young's modulus can be achieved. An optimization of hollow sphere thickness in MSF may be required for practical manufacturing of metallic hollow spheres. In addition, the data point (denoted by an unfilled square) from tomography based models that resembles the thin walled MSF is in line with those for thin walled MSF, and is similar to the value obtained for a pure epoxy matrix (denoted by star maker). Further, an experimental value (denoted by sun-shaped marker) for similar (thick-walled) MSF elsewhere [44] appears to be in good agreement with numerical findings, supporting the validity of the numerical modeling.

Poisson's ratio ($\nu$) may not be a major parameter for the optimum design of light weight structures. However, it is important for understanding of deformation, given that it is an elastic parameter relating between different elastic moduli. When the three different cases are considered, it is expected that the zero walled case (porous material) would be low for Poisson's ratio compared to thin and thick walled MSFs. The reason is that the structural deformation with only pores in transverse direction to the loading direction would be relatively small compared to the structures with hollow spheres for a given volume fraction of matrix, given that the deformation around a pore in the absence of sphere wall tends to be more collapsible than around a sphere. In *Fig. 8* numerical data sets obtained for Poisson's ratio ($\nu$) from the three different cases are given as a function of volume fraction of matrix. It can be seen that there is an obvious difference in Poisson's ratio between the zero walled case and MSF with hollow spheres. This supports the expected deformation dis-

 

cussed here and thus they also support the validity of the finite element analysis. Further, not much difference between thin and thick walled MFSs is found, indicating that Poisson's ratio is not sensitively affected by the hollow sphere wall thickness within the range given in this work.

## 6 Conclusion

Elastic finite element analysis using 2D models based on cross sections of metallic hollow sphere structures has been performed. Elastic parameters for hollow sphere wall material, metallic syntactic foams (MSF) consisting of thin or thick walled hollow spheres, and for epoxy containing spherical pores are calculated and compared with theoretical predictions developed elsewhere. The data obtained are found to be in good agreement with theoretical predictions for metallic syntactic foams except for porous material containing no hollow spheres.

In addition, the following findings from the finite element analyses are addressed within the data range employed.

1. The Young's modulus ($E$) of metallic hollow sphere wall material linearly decreases with increasing micro-porosity ranging up to about 45%.
2. The shear modulus of MSF with thin walled hollow spheres increases with increasing volume fraction of matrix whereas the shear modulus of MSF with thick walled hollow spheres decreases.
3. The specific Young's modulus of MSF with thin walled hollow spheres increases with increasing foam density whereas that of MSF with thick walled hollow spheres decreases.
4. Poisson's ratio is low for porous epoxy matrix material but high for MSF with thin and thick walled hollow spheres.

## 7 References


[1] H. S. Kim, M. A. Khamis, *Compos. Part A – Appl. S.* **2001**, *32A*, 1311.

[2] H. S. Kim, *J. Appl. Polym. Sci.* **2007**, *105*, 3287.

[3] N. N. Jize, C. Hiel, O. Ishai, "Mechanical Performance of composite sandwich beams with syntactic foam cores", R. B. Deo and C. R. Saff, (Eds), ASTM STP 1274, **1996**, pp.125–138.

[4] L. K. English, *Mater. Eng.* **1987**, *4*, 51.

[5] D. Jackson, P. Clay, *Sea Technol.* **1983**, *24*, 29.

[6] P. W. Harruff, B. E. Sandman, presented at 28th National SAMPE Symposium, Anaheim CA, April 12–14, **1983**, pp.40–49.

[7] L. Watkins, presented at the Seventh International Conference on Offshore Mechanical and Artic Engineering, Houston, Texas, Feburuary 7–12, **1988**, pp.403–410.

[8] M. J. Seamark, *Cell. Polym.* **1991**, *10*, 308.

[9] J. B. Hinves, C. D. Douglas, IEEE, **1993**, pp.III–468–472.

[10] H. S. Kim, P. Plubrai, *Compos. Part A – Appl. S.* **2004**, *35*, 1009.

[11] K. S. Young, *Mod. Plast.* **1985**, April, 92.

[12] M. Narkis, M. Gerchcovich, M. Puterman, S. Kenig, *J. Cell. Plast.* **1982**, July/August, 230.

[13] M. Narkis, M. Puterman, H. Boneh, *Polym. Eng. Sci.* **1982**, *22*, 417.

[14] E. Lawrence, D. Wulfsohn, R. Pyrz, *Polym. Polym. Compos.* **2001**, *9*, 449.

[15] E. Lawrence, R. Pyrz, *Polym. Polym. Compos.* **2001**, *9*, **227.**

[16] H. Verweij, G. De With, D. Veeneman, *J. Mater. Sci.* **1985**, *20*, 1069.

[17] M. Narkis, M. Puterman, S. Kenig, *J. Cell. Plast.* **1980**, Nov–Dec, 326.

[18] M. Puterman, M. Narkis, *J. Cell. Plast.* **1980**, July/August, 223.

[19] S. Kenig, I. Raiter, M. Narkis, *J. Cell. Plast.* **1984**, Nov–Dec, 423.

[20] C. Meter, *International patent*, WO 97/29900, **1997**.

[21] H. S. Kim, H. H. Oh, presented at The first ACUN International Composites Meeting on Composites : Innovation and Structural Applications, University of New South Wales, Sydney, Australia, 23–25 February, **1999**, pp. 83–86.

[22] H. S. Kim, H. H. Oh, *J. Appl. Polym. Sci.* **2000**, *76*, 1324.

[23] K. te Nijenhuis, R. Addink, A. K. van der Vegt, *Polym. Bull.* **1989**, *21*, 467.

[24] H. S. Kim, International Patent C08J 9/32, **2003**.

[25] H. S. Kim, International Patent, WO 2006/005119 A1, **2006**.

[26] A. Daoud, *Mater. Sci. Eng A – Struct.* **2008**, *488*, 281.

[27] P. K. Rohatgi, R. Q. Guo, H. Iksan, E. J. Borchelt, R. Asthana, *Mater. Sci. Eng A – Struct.* **1998**, *244*, 22.

[28] O. Andersen, U. Waag, L. Schneider, G. Stephani, B. Kieback, *Adv. Eng. Mater.* **2000**, *2*, 192.

[29] T. Fiedler, R. Löffler, T. Bernthaler, R. Winkler, I. V. Belova, G. E. Murch, A. Öchsner, *Mater. Lett.* **2009**, *63*, 1125.

[30] T. Fiedler, A. Öchsner, I. V. Belova, G. E. Murch, *Defect Diffus. Forum* **2008**, *273–276*, 216.

[31] T. Fiedler, A. Öchsner, *Scripta Mater.* **2008**, *58*, 695.

[32] T. J. Lim, B. Smith, D. L. McDowell, *Acta Mater.* **2002**, *50*, 2867.

[33] H. S. Kim, P. Plubrai, *Compos. Part A – Appl. Sci.* **2004**, *35*, 1009.

[34] H. S. Kim, M. Islam, "Syntactic foams as building materials consisting of inorganic hollow microspheres and starch binder", in Building Materials: Properties and Performance and Applications, Edited by Donald N. Cornejo and Jason L. Haro, Nova publishers, in press, **2009**.

[35] M. Islam, H. S. Kim, *J. Mater. Sci.* **2007**, *42*, 6123.

[36] M. Kaczmarek, M. Goueygou, *J. Porous Media* **2006**, *9*, 1.

[37] R. Pal, *Compos. Part B – Eng.* **2006**, *36*, 513.

[38] R. M. Christensen, *J. Mech. Phys. Solids* **1990**, *38*, 379.

[39] Q. Chen, A. Nur, "Chapter 4 – Critical concentration models for porous materials", pp. 169–308. in Advances in Porous Media, Ed. by M. Yavuz Corapcioglu, Volume 2, Elsevier, Amsterdam. London, New York, Tokyo, **1994**.

[40] J. D. Eshelby, *P. Roy. Soc. A – Math. Phys.* **1957**, *241*, 376.

[41] N. H. Kim, H. S. Kim, *J. Appl. Polym. Sci.* **2005**, *98*, 1290.

[42] C. Veyhl, M. Merkel, A. Öchsner, *Defect Diffus Forum* **2008**, *280–281*, 105.

[43] N. H. Kim, H. S. Kim, *J. Appl. Polym. Sci.* **2005**, *98*, 1663.

[44] T. Fiedler, Numerical and Experimental Investigation of Hollow Sphere Structures in Sandwich Panels, Trans Tech Publications, Zuerich **2008**.


Received in final form: March 31st 2010 T 593

 